

## Electronic Supplementary Information

### Creating supramolecular semiregular Archimedean tilings via gas-mediated deprotonation of a terminal alkyne derivative

Wenqi Hu,<sup>a,b</sup> Hexu Zhang,<sup>a,b</sup> Peng Cheng,<sup>a,b</sup> Lan Chen,<sup>a,b</sup> Zhi Chen,<sup>c</sup> Svetlana  
Klyatskaya,<sup>c</sup> Mario Ruben,<sup>\*,c,d,e</sup> Johannes V. Barth,<sup>\*,f</sup> Kehui Wu,<sup>\*,a,b</sup> and Yi-Qi  
Zhang,<sup>\*,a</sup>

<sup>a</sup> *Institute of Physics, Chinese Academy of Sciences, Beijing 100190, China*

*E-mail: yiqi.zhang@iphy.ac.cn; khwu@iphy.ac.cn*

<sup>b</sup> *School of Physical Sciences, University of Chinese Academy of Sciences, Beijing  
100049, China*

<sup>c</sup> *Institute of Nanotechnology, Karlsruhe Institute of Technology, 76344 Eggenstein-  
Leopoldshafen, Germany*

<sup>d</sup> *Institute for Quantum Materials and Technologies (IQMT), Karlsruhe Institute of  
Technology (KIT), Hermann-von-Helmholtz-Platz 1, 76344, Eggenstein-  
Leopoldshafen, Germany*

<sup>e</sup> *Centre Européen de Sciences Quantiques (CESQ), Institut de Science et d'Ingénierie  
Supramoléculaires (ISIS), 8 allée Gaspard Monge, BP 70028, 67083 Strasbourg  
Cedex, France*

*E-mail: mario.ruben@kit.edu*

<sup>f</sup> *Physics Department E20, Technical University of Munich, D-85748 Garching,  
Germany*

*E-mail: jvb@tum.de*

## Index

Ethynyl-phenanthrene (EP) molecules adsorbed on Ag(111)/mica	Figure S1
Large-scale STM images of three ordered phases	Figure S2
Noncovalent molecular interactions among BPE-Ag units	Figure S3
$\rho$ -domain of Kagome phase 1 (P1)	Figure S4
$\rho$ -domain of Kagome phase 2 (P2)	Figure S5
$\rho$ -domain of the (3.4.6.4) AT phase (P3)	Figure S6
The distribution of BPE-Ag dimer configurations	Figure S7
Estimation of the conversion yield from EP molecules to BPE-Ag species	
References	

## Ethynyl-phenanthrene (EP) molecules adsorbed on Ag(111)/mica

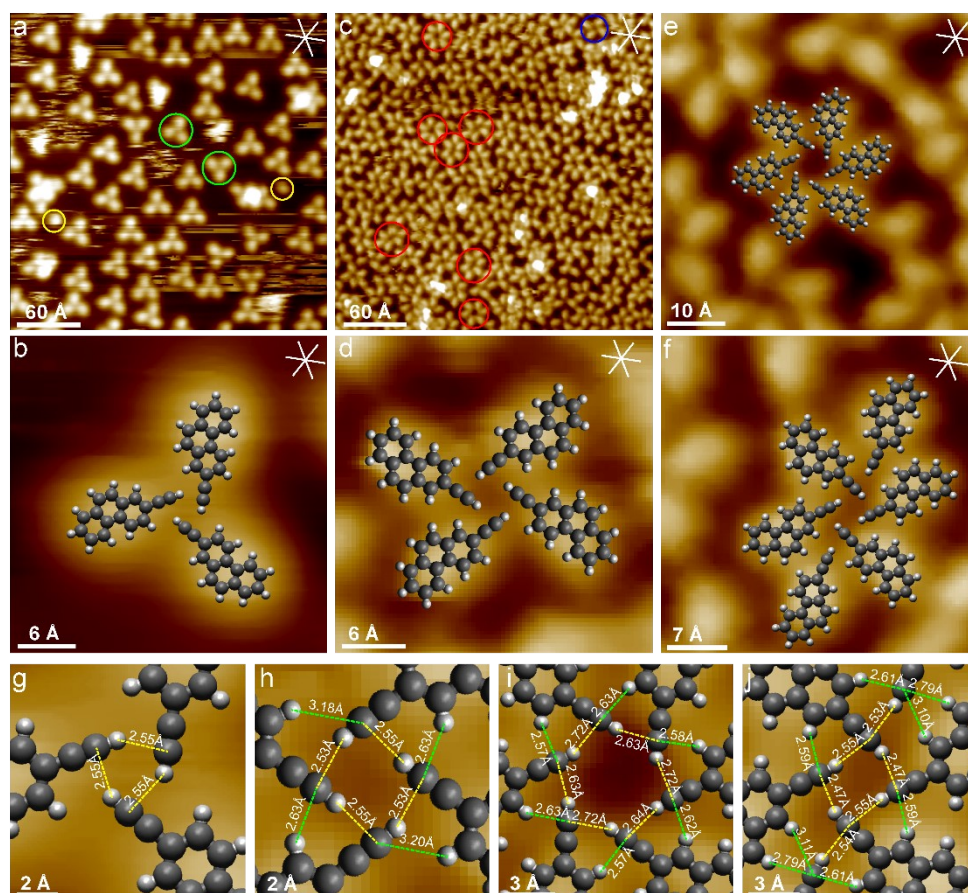


Figure S1. (a) Large-scale STM image of low-coverage EP molecules grown on Ag(111)/mica at RT.  $I_t = 30$  pA,  $U_s = 1.0$  V. (b) Magnified STM image of a trimer superimposed with ball-and-stick models.  $I_t = 30$  pA,  $U_s = 1.0$  V. (c) Large-scale STM image of EP molecules grown on Ag(111)/mica at RT with increased coverage.  $I_t = 50$  pA,  $U_s = 1.0$  V. Magnified STM images of a tetramer (d), two hexamers (e, f) superimposed with ball-and-stick models. Zoomed-in bonding geometries: (g) trimer shown in (b); (h) tetramer in (d); (i) regular hexamer in (e); (j) irregular hexamer in (f). The C–H···C distances in the bonding motifs are displayed. The isolated monomer, trimers, tetramers and hexamers, are highlighted using circles of different colours.

The molecular arrangements in clusters of different sizes were assessed via a simplified density functional theory (DFT) modelling, describing EP molecules in the gas-phase (cf. Methods) imposing in-plane constraint. Van der Waals interactions are taken into account by including the D3BJ correction. The bonding motifs present in the trimer, tetramer and regular hexamers mimic those observed in our previous

studies, indicating the weak C–H $\cdots$  $\pi$  interaction<sup>1</sup> between the terminal alkynes. Although the geometry of the synthon presented in Figure S1f deviates from the more regular cyclic organization, it can also be reproduced by the gas-phase calculation with intact EP molecules. Moreover, a similar arrangement was also observed for intact phenylacetylene molecular clusters adsorbed on Au(111)<sup>2</sup>.

## Large-scale STM images of three ordered phases

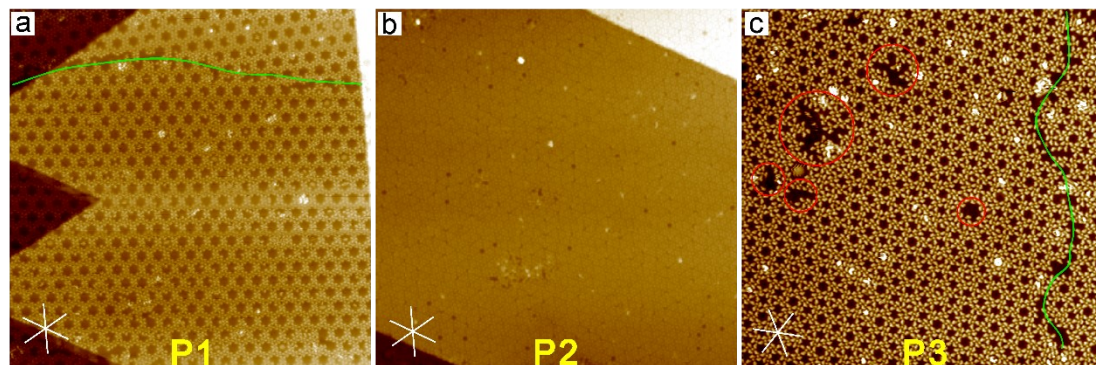


Figure S2. Large-scale STM images of three different types of porous phases: (a) P1 phase ( $100 \times 100 \text{ nm}^2$ ), (b) P2 phase ( $100 \times 100 \text{ nm}^2$ ), (c) P3 phase ( $60 \times 60 \text{ nm}^2$ ). High-symmetry directions of the Ag(111) surface are indicated. Green curves indicate the edges of the domains and red cycles highlight the defects. Scanning parameters for all images are:  $I_t = 30 \text{ pA}$ ,  $U_s = 1.0 \text{ V}$ .

For three different types of nanoporous networks, P1 and P2 exhibit long-range order ( $> 100 \text{ nm}$ ), whereas P3 shows a shorter ordered distance ( $\sim 60 \text{ nm}$ ) and is more vulnerable to defects.

## Noncovalent molecular interactions among BPE-Ag units

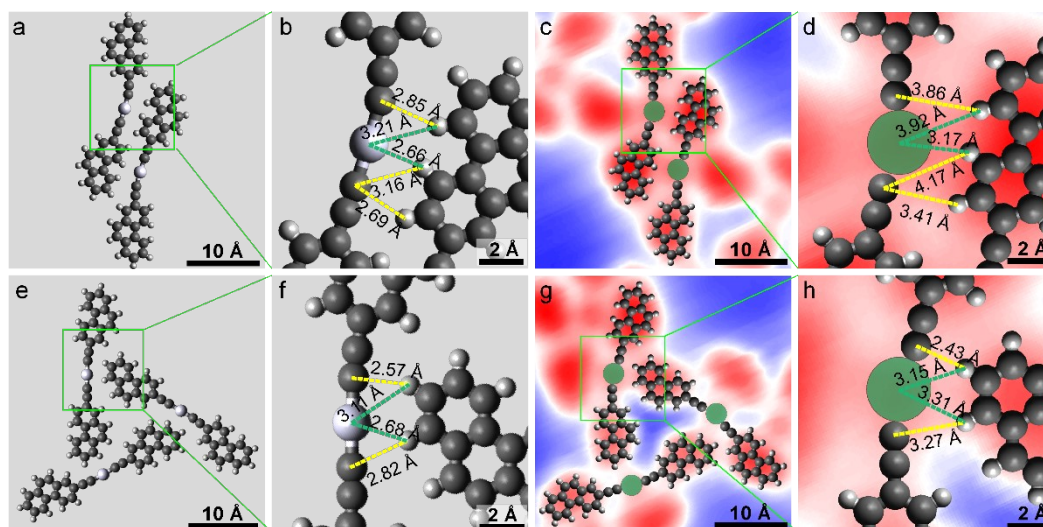


Figure S3. (a) BPE-Ag organometallic dimer geometry obtained from the DFT gas-phase modelling. (b) Zoomed-in image of (a) showing the calculated noncovalent C-H...Ag and C-H...C distances. (c) BPE-Ag dimer configuration derived from a corresponding STM image.  $I_t = 30$  pA,  $U_s = 1.0$  V. (d) Zoomed-in image of (c) showing the derived noncovalent C-H...Ag and C-H...C distances. (e) BPE-Ag organometallic trimer obtained from DFT gas-phase simulation. (f) Zoomed-in image of (e) with calculated noncovalent C-H...Ag and C-H...C distances. (g) BPE-Ag trimer arrangement derived from a corresponding STM image.  $I_t = 30$  pA,  $U_s = 1.0$  V. (h) Zoomed-in image of (g) showing the derived noncovalent C-H...Ag and C-H...C distances.

Organometallic BPE-Ag dimer and trimer self-assembly configurations were examined via DFT gas-phase calculations with in-plane constraint (cf. Methods) and the van der Waals interactions are included using the D3BJ correction. The calculated distances between the hydrogen atoms from the phenanthrene backbone to the alkynyl-Ag atom as well as to the ethynyl-carbon atoms fall into the category of hydrogen bonds, indicating the electron-rich character of the transition metal<sup>3-5</sup> as well as the alkynyl  $\pi$ -systems<sup>6, 7</sup>(Figure S3b,f). The discrepancies exhibiting in the hydrogen bonding distances between the modelling and the derived experimental values are presumably ascribed to the following reasons: (i) the missing interaction with the substrate in the gas-phase calculations; (ii) the oversimplified and isolated

interaction scheme shown in (a,e); (iii) possible out-of-plane tilting of the phenanthrene backbones.

### $\rho$ -domain of Kagome phase 1 (P1)

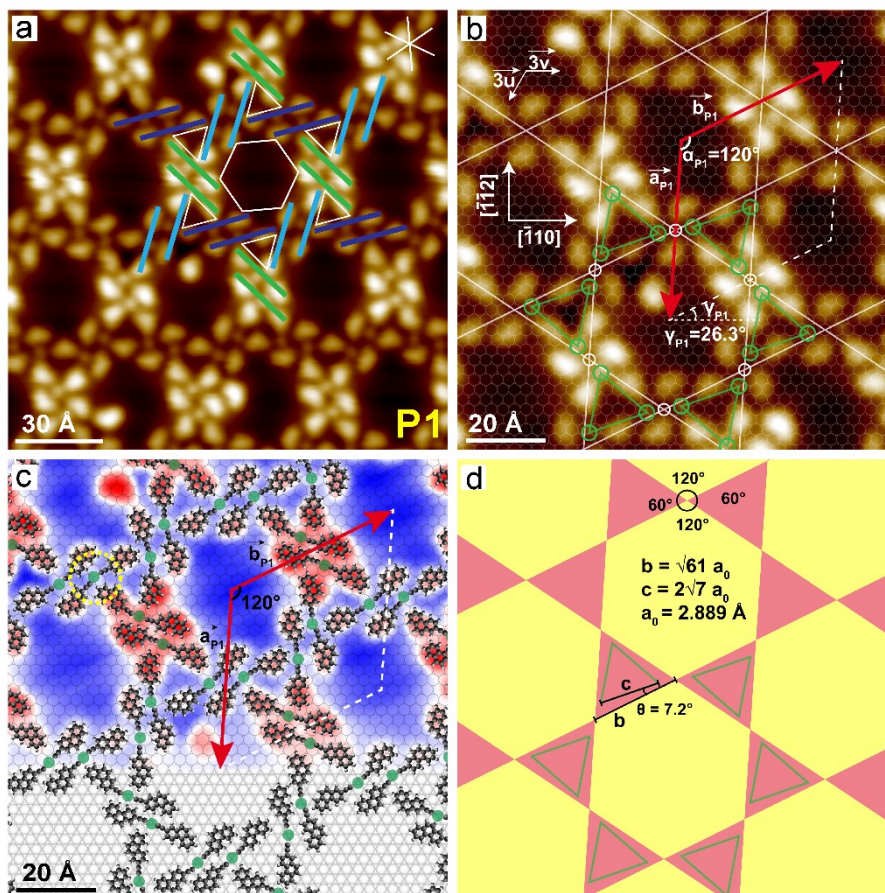


Figure S4. (a) High-resolution STM image for the  $\rho$ -domain of the P1 phase. The white hexagon and triangles highlight the nanopore enclosed by the BPE-Ag molecules.  $I_t = 30$  pA,  $U_s = 1.0$  V. (b) Magnified STM image of (a) with a commensurate unit cell and proposed registry. Green circles highlight alkynyl-Ag nodes, whereas white lines featuring the Kagome (3.6.3.6) AT are defined via linking the midpoints (white circles) of the BPE-Ag pairs. (c) STM image of figure (b) with proposed molecular registry. (d) Tiling representation of (b) with geometric parameters. Green triangles are obtained via linking three Ag nodes residing in the triangular tile.

Figure S4 illustrate the  $\rho$ -domain<sup>8, 9</sup> of the P1 phase. The experimentally determined values for the unit cell are  $|\vec{a}_{P1}'| = 44.8 \pm 0.2$  Å,  $|\vec{b}_{P1}'| = 44.7 \pm 0.3$  Å, and  $\alpha_{P1}' = 60.4 \pm 0.6^\circ$  (cf. Figure S4b). The angle  $\gamma_{P1}'$  equals  $26.3 \pm 0.1^\circ$ . Accordingly, its

commensurate model can be written as:

$$\begin{pmatrix} \vec{a}_{P1} \\ \vec{b}_{P1} \end{pmatrix} = \begin{pmatrix} 18 & 8 \\ -8 & 10 \end{pmatrix} \begin{pmatrix} \vec{u} \\ \vec{v} \end{pmatrix}$$

, which gives  $|\vec{a}_{P1}| = |\vec{b}_{P1}| = 2\sqrt{61} a_0 = 45.13 \text{ \AA}$ ,  $\alpha_{P1} = 60^\circ$ , and  $\gamma_{P1} = 26.3^\circ$ . A nice agreement has been reached between the model and the experimental findings within an error smaller than 1.0%.

The molecular adsorption registries in both  $\lambda$  and  $\rho$ -domains share the same characteristics (cf. Figure S4c and Figure 2c) and the Kagome tilings extracted from enantiomorphic domains have mirror symmetry with respect to the  $[1\bar{1}2]$  and the  $[110]$  directions.

$\rho$ -domain of Kagome phase 2 (P2)

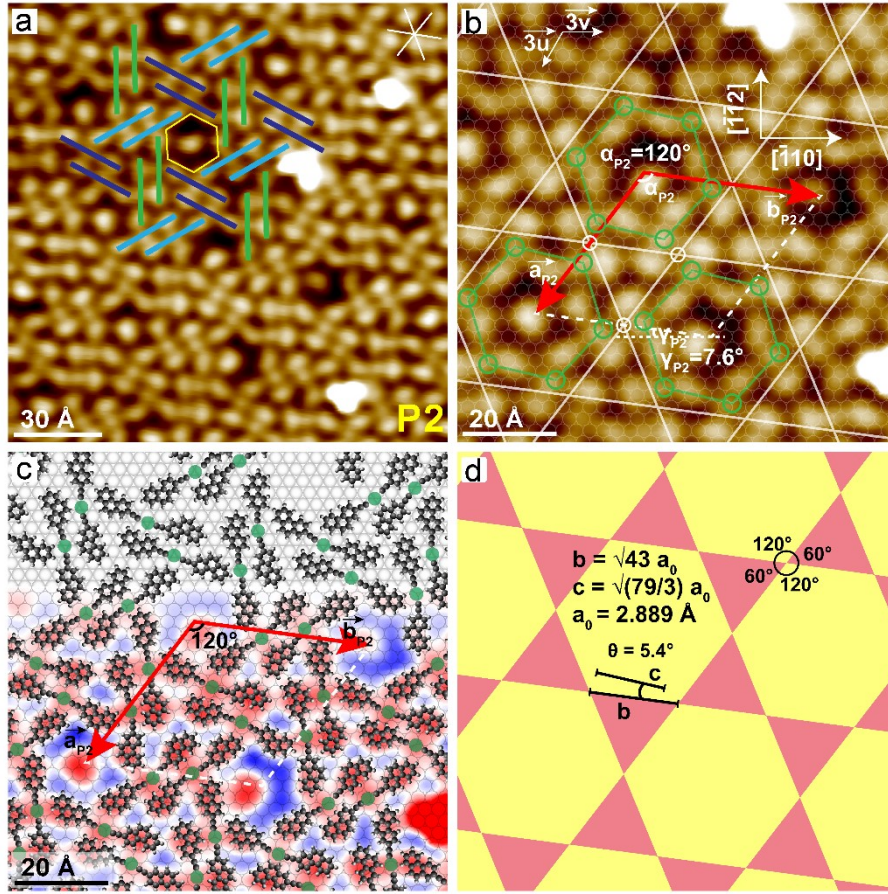


Figure S5. (a) High-resolution STM image for the  $\rho$ -domain of P2. The yellow hexagon highlights the nanopore enclosed by six BPE-Ag monomers.  $I_t = 50$  pA,  $U_s = 0.1$  V. (b) Magnified STM image of (a) with a commensurate unit cell model and proposed registry. Green circles highlight the alkynyl-Ag nodes, whereas white circles are defined at the midpoints between Ag nodes, which lead to the Kagome (3.6.3.6) AT. (c) STM image of (b) superposed with molecular registry. (d) Tiling representation of (b) with geometric parameters. Green hexagons in (b) and (d) are created via linking the Ag nodes within the large hexagonal tile.

A statistical analysis of experimental data of the  $\rho$ -domains of P2 yielded  $|\vec{a}'_{P2}| = 37.9 \pm 0.2$  Å,  $|\vec{b}'_{P2}| = 37.9 \pm 0.6$  Å and  $\alpha'_{P2} = 60.0 \pm 0.7^\circ$ . The angle  $\gamma'_{P2}$  between  $\vec{b}'_{P2}$  and one of the  $[110]$  high-symmetry directions (horizontal direction in Figure S5b) is  $8.1 \pm 0.3^\circ$ . Hence, a commensurate unit cell can be constructed:

$$\begin{pmatrix} \vec{a}_{P2} \\ \vec{b}_{P2} \end{pmatrix} = \begin{pmatrix} 12 & -2 \\ 2 & 14 \end{pmatrix} \begin{pmatrix} \vec{u} \\ \vec{v} \end{pmatrix}$$

, with  $|\vec{a}_{P2}| = |\vec{b}_{P2}| = 2\sqrt{43}$   $a_0 = 37.89$  Å,  $\alpha_{P2} = 60^\circ$ , and  $\gamma_{P2} = 7.6^\circ$ , which are comparable to the experimental values within an error smaller than 0.9 %.

For the P2 phase, the molecular adsorption configurations in mirror domains bear similar characteristics and the tiling patterns present mirror symmetry with respect to the  $[\bar{1}\bar{1}2]$  and the  $[\bar{1}10]$  directions.

$\rho$ -domain of the (3.4.6.4) AT phase (P3)

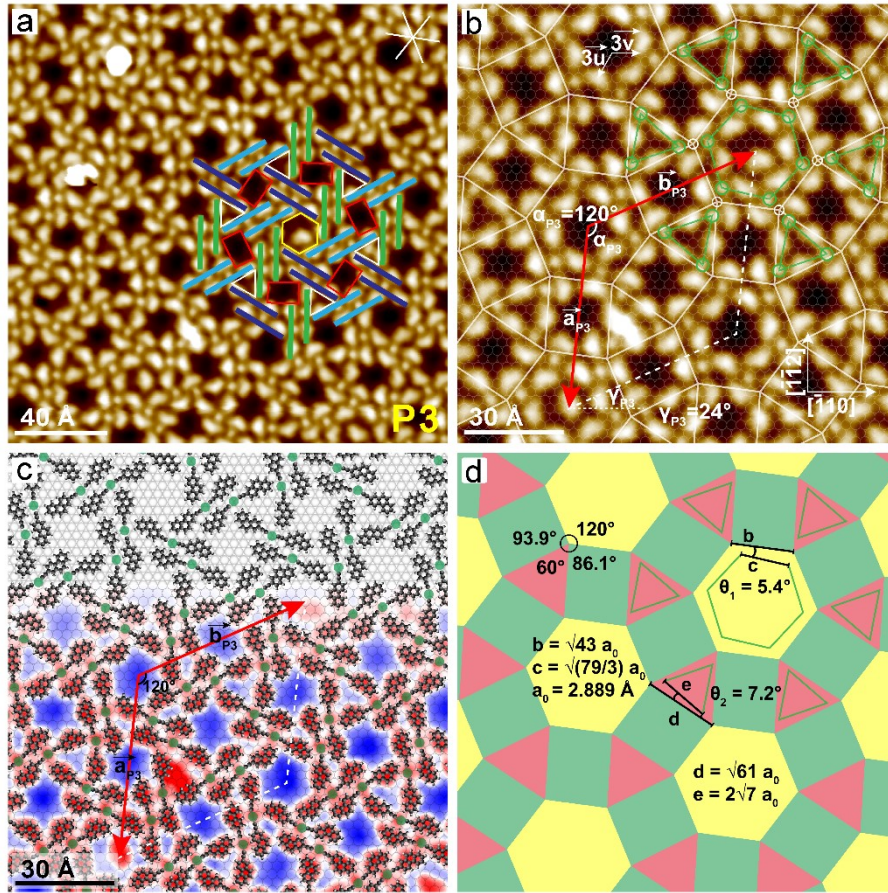


Figure S6. (a) High-resolution STM image of the  $\rho$ -domain of P3. The yellow hexagon, triangles and red rectangles highlight the nanopores enclosed by the BPE-Ag species.  $I_t = 50$  pA,  $U_s = 1.0$  V. (b) Magnified STM image of (a) with a commensurate unit cell model and proposed registry. Green circles highlight the alkyne-Ag nodes, whereas the white circles defined at the midpoints between the Ag nodes give rise to the (3.4.6.4) AT. (c) STM image of (b) superposed with molecular registry. (d) Tiling representation of (b) with geometric parameters.

The measured values for the  $\rho$ -domain of P3 are  $|\vec{a}_{P3}| = 54.7 \pm 0.4$  Å,  $|\vec{b}_{P3}| = 54.8 \pm 1.4$  Å and  $\alpha_{P3} = 60.5 \pm 0.4^\circ$ . The angle  $\gamma_{P3}$  equals  $23.9 \pm 0.4^\circ$ . The corresponding

$$\begin{pmatrix} \vec{a}_{P3} \\ \vec{b}_{P3} \end{pmatrix} = \begin{pmatrix} 22 & 9 \\ -9 & 13 \end{pmatrix} \begin{pmatrix} \vec{u} \\ \vec{v} \end{pmatrix}$$

commensurate unit cell can be expressed as:

, which gives  $|\vec{a}_{P3}| = |\vec{b}_{P3}| = \sqrt{367} a_0 = 55.35$  Å,  $\alpha_{P3} = 60^\circ$ , and  $\gamma_{P3} = 24^\circ$ , within an

error of approximately 1.2 %.

The molecular adsorption registries in both  $\lambda$  and  $\rho$ -domains for the P3 phase are similar and the tiling patterns for the enantiomorphic domains present mirror symmetry with respect to the  $[\bar{1}\bar{1}2]$  and the  $[\bar{1}10]$  directions.

## The distribution of BPE-Ag dimer configurations

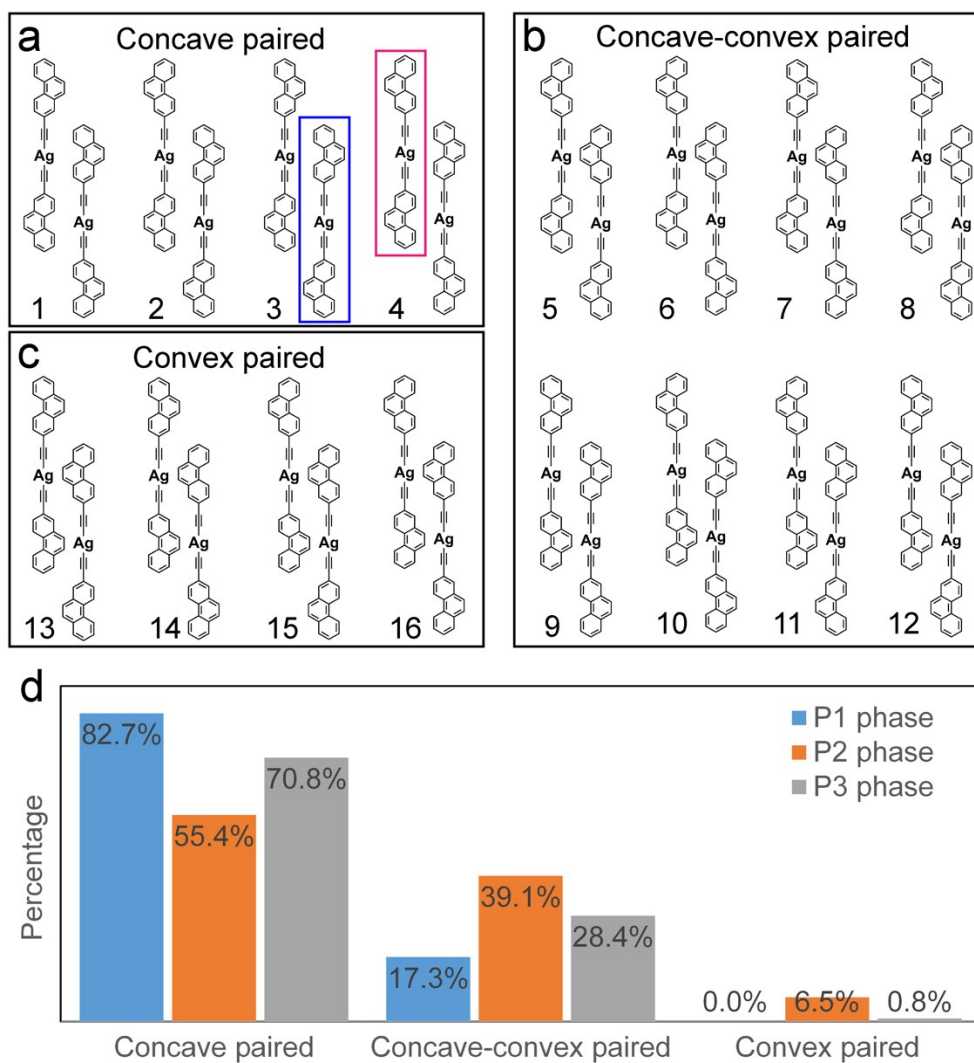


Figure S7. (a-c) Configurations for *concave* paired, *concave-convex* paired and *convex* paired BPE-Ag dimers, respectively. Red and blue rectangles highlight the *cis* and *trans* conformers, respectively. (d) The distribution of dimer configurations with respect to each phase.

The concave or convex configuration is defined according to the edge curvature of the EP molecule that is pointing towards the alkynyl-Ag atom (cf. Figure. S7a-c).

## Estimation of the conversion yield from EP molecules to BPE-Ag species

For the P1 phase, there are 12 EP molecules forming the BPE-Ag complexes in one unit-cell and 13 EP molecules in total, if we assume that the hexagonal cage is occupied. Therefore, we estimate that the minimum conversion from EP to BPE-Ag has a yield of  $12/13 \approx 92\%$ . For P2 phase, in a similar manner, we obtained that the conversion yield from EP to BPE-Ag species is  $12/13 \approx 92\%$  at least, same as that of P1. The elementary cell of the P3 phase contains 24 EP molecules forming the BPE-Ag complexes and 25 EP molecules in total, taking one EP molecule trapped in the hexagonal cage into account. Therefore, the EP to BPE-Ag transition yield shall be larger than  $24/25 \approx 96\%$ . Hence, we conclude that oxygen-gas mediated terminal alkyne deprotonation reaction can convert EP molecules to BPE-Ag molecules with a yield higher than 92%.

In our first report<sup>10</sup> of the oxygen-gas mediated terminal alkyne deprotonation reaction, we could quantify the deprotonation rate of 1,3,5-tris(4-ethynylphenyl)benzene (Ext-TEB) molecules at  $T_{\text{sub}} = 200$  K to be  $\sim 95\%$  employing X-ray photoelectron spectroscopy (XPS)<sup>10</sup>. As the same reaction was applied to EP molecules adsorbed on Ag(111)/mica at RT, we would assume a similar deprotonation rate for EP molecules, which is reconciled with the estimated EP conversion rate of 92%.

## REFERENCES

1. T. Lin, Y.-Q. Zhang, L. Zhang and F. Klappenberger, *Encyclopedia of Interfacial Chemistry: Surface Science and Electrochemistry*, 2017, **3**, 55-66.
2. Q. Li, C. Han, S. R. Horton, M. Fuentes-Cabrera, B. G. Sumpter, W. Lu, J. Bernholc, P. Maksymovych and M. Pan, *Acs Nano*, 2012, **6**, 566-572.
3. L. Brammer, D. Zhao, F. T. Ladipo and J. Braddock-Wilking, *Acta Crystallogr. Sect. B*, 1995, **51**, 632–640.
4. D. Braga, F. Grepioni and G. R. Desiraju, *Chem. Rev.*, 1998, **98**, 1375-1406.
5. T. Steiner, *Angew. Chem. Int. Ed.*, 2002, **41**, 48-76.

6. Y.-Q. Zhang, J. Björk, P. Weber, R. Hellwig, K. Diller, A. C. Papageorgiou, S. C. Oh, S. Fischer, F. Allegretti, S. Klyatskaya, M. Ruben, J. V. Barth and F. Klappenberger, *J. Phys. Chem. C*, 2015, **119**, 9669.
7. Y.-Q. Zhang, M. Paszkiewicz, P. Du, L. Zhang, T. Lin, Z. Chen, S. Klyatskaya, M. Ruben, A. P. Seitsonen, J. V. Barth and F. Klappenberger, *Nat. Chem.*, 2018, **10**, 296-304.
8. R. Raval, *Chem. Soc. Rev.*, 2009, **38**, 707-721.
9. K. H. Ernst, *Phys. Status Solidi B*, 2012, **249**, 2057-2088.
10. Y.-Q. Zhang, T. Paintner, R. Hellwig, F. Haag, F. Allegretti, P. Feulner, S. Klyatskaya, M. Ruben, A. P. Seitsonen, J. V. Barth and F. Klappenberger, *J. Am. Chem. Soc.*, 2019, **141**, 5087-5091.